CCFE
CULHAM CENTRE FOR FUSION ENERGY

UK Atomic Energy Authority

UKAEA-CCFE-PR(20)139

J.M. Gao, L.Z. Cai, X.L. Zou, T. Eich, C.Z Cao, L.W. Yan, W.L. Zhong, A.J. Thornton, J. Adamek, X.Q. Ji, M. Jiang, L. Liu, J. Lu, G.L. Xiao, Z.H. Huang, N. Wu

Type I ELM power loads on the closed outer divertor targets in the HL2A tokamak

Type I ELM power loads on the closed outer divertor targets in the HL2A tokamak

J.M. Gao, L.Z. Cai, X.L. Zou, T. Eich, C.Z Cao, L.W. Yan, W.L. Zhong, A.J. Thornton, J. Adamek, X.Q. Ji, M. Jiang, L. Liu, J. Lu, G.L. Xiao, Z.H. Huang, N. Wu

This is a preprint of a paper submitted for publication in Nuclear Fusion

Type-I ELM power loads on the closed outer divertor targets in the HL-2A tokamak

J.M. Gao[1], L.Z. Cai[1], X.L. Zou[2], T. Eich[3], C.Z Cao[1], L.W. Yan[1], W.L. Zhong[1], A.J. Thornton[4], J. Adamek[5], X.Q. Ji[1], M. Jiang[1], L. Liu[1], J. Lu[1], G.L. Xiao[1], Z.H. Huang[1], N. Wu[1], L.M. Yu[1], Y. Liu[1], D.L. Yu[1], X.M. Song[1], Q.W. Yang[1], Z.B. Shi[1], M. Xu[1], and the HL-2A team[1].

[1]Southwestern Institute of Physics, Chengdu 610041, People's Republic of China
[2]CEA, IRFM, Saint-Paul-lez-Durance F-13108, France
[3]Max-Planck-Institut für Plasmaphysik, Garching, Germany
[4]CCFE, Culham Science Centre, Oxfordshire OX14 3DB, United Kingdom
[5]Institute of Plasma Physics of the CAS, Prague, Czech Republic

E-mail: gaojm@swip.ac.cn

Abstract

The HL-2A tokamak has a very closed divertor geometry, and a new infrared camera has been installed for high resolution studies of edge-localized mode (ELM) heat load onto the outer divertor targets. The characteristics of power deposition patterns on the lower outer divertor target plates during ELMs are systematically analyzed with the infrared thermography. The ELM energy loss is in the range of 3-8% of the total plasma stored energy. The peak heat flux on the outer divertor targets during ELMs currently achieved in HL-2A is about *1.5-3.2MWm*$^{-2}$, the wetted area is about 0.5-0.7m^2, and the corresponding integrated power decay length at the midplane is about 25-*40mm*. The rise time of the ELM power deposition is in the range of about $100\mu s$ to $400\mu s$, and the decay time is typically 1.5 to 4 times longer than the corresponding rise time. Convective transport along open field lines during ELMs from the midplane towards the divertor targets is implied due to the correlation of parallel transport time in the SOL and ELM power rise time. The peak ELM energy fluence is compared with those predicted by model and with experimental data from JET, ASDEX-Upgrade, MAST and COMPASS. The results, as a whole, show a good agreement.

1. Introduction

Operation in H-mode is considered to be the reference scenario for next step tokamak devices, such as ITER [1]. The H-mode plasmas are affected by quasi-periodic MHD instabilities occurring at the edge transport barrier region named Edge Localized Modes (ELMs) [2,3]. The ELM causes a sudden crash of the transport barrier with transient releases of energy and particles into the scrape-off layer (SOL) and eventually moves towards the divertor [4]. The resulting high heat load deposited onto the divertor targets may pose a serious threat to the devices. Therefore, understanding the divertor heat load patterns during ELMs is an important issue for handing the high energy flux. Considerable efforts have been dedicated to understand the behaviour of divertor heat flux during ELMs in JET [5], ASDEX Upgrade [6], DIII-D [7], EAST [8], and so on. It is found that during ELMs about 1-30% of the plasma stored energy is released within a few hundred microseconds towards the divertor, and the power decay length (deposited area) is only tens of millimeters. Extrapolation of the multi-machine experimental results to ITER indicates the parallel peak ELM energy fluence is of 2.5-7.5MJ for the intermediate ITER operation at 7.5MA and 2.65T [9]. It is larger than the material limit for ELM peak divertor thermal impact. Thus, ELM control techniques, such as resonant magnetic perturbations and impurity seeding, could be required for next step tokamak devices.

The ELM mitigation requirements are based on extrapolations which depend on models. Based on experimental findings on JET, ASDEX Upgrade, and MAST, a model was put forward, from here on referred to as the Eich model [9]. The Eich model proposes that parallel ELM energy densities scale with pedestal pressure, and the predictions are compared against a multi-machine dataset, including measurements from JET, ASDEX Upgrade, and MAST [9]. The scaling prediction is recently tested on COMPASS [10] and DIII-D [11] with a good agreement.

The HL-2A tokamak has a very closed divertor geometry, and the outer divertor target plates are monitored with a fast infrared (IR) camera. A set of ELMy H-mode discharges has been performed during the HL-2A divertor campaign with an optimized divertor configuration, so that the outer strike point is located in the field of view of the IR camera [12,13]. The power deposition characteristics of type-I ELMs with frequency from 70Hz to 200Hz are investigated with the IR camera. The energy loss during ELMs currently achieved in HL-2A is in the range of 3% to 8% of the total plasma stored energy, as a result, the peak heat flux on the outer divertor targets is about $1.5\text{-}3.2 MWm^{-2}$, and the integrated power decay length at the midplane is about *25-40mm*. During the ELM cycle, the decay time is much larger than the rise time, and the rise time is comparable to the parallel transport time in the SOL. Finally, the ELM energy density profiles and peak ELM energy density values are compared to the scaling predictions from ASDEX Upgrade, JET, MAST, and COMPASS.

The rest of this paper is organized as follows. In section 2, a brief description of the HL-2A divertor configuration, ELM diagnostic systems and the ELMy H-mode plasma data base, is given. Characteristics of the ELM power load on the outer divertor targets are reported in sections 3. Section 4 presents the energy transport in the SOL during ELMs. The ELM energy density profiles and the peak ELM energy fluence are compared to the scaling predictions from JET, ASDEX-Upgrade, MAST and COMPASS in section 5. Finally, summary and conclusions

are drawn in section 6.

2. Experimental arrangement

2.1 Divertor configuration

The HL-2A tokamak (major radius $R=1.65m$ and minor radius $a=0.4m$) has a double-null divertor with a very closed divertor geometry, where a closely spaced coil triplet with zero net current is used to produce the divertor configuration [13], as shown in figure 1. Additional ("multipole compensation") coils are added to cancel even the residual far-field of the two (symmetrically top and bottom) divertor triplets over the main plasma region, so that core flux surfaces are close to perfectly circular. The poloidal flux surfaces in the lower divertor region show that the flux expansion is approximately by a factor of 2-3 between the divertor throat and the target plate region for the flux surfaces in the separatrix proximity. As a side effect, this physically closed divertor geometry also allows for an efficient baffling of the neutral particles and a reduction of the back-streaming into the main chamber. These effects lead to an enhancement of plasma radiation loss in the divertor plasma, and thus offer a possibility to mitigate the heat flux deposited onto the target plates.

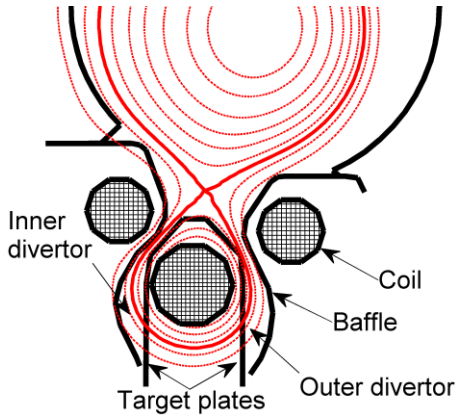

Figure 1. Coils, baffles and target plates form the very closed lower divertor of HL-2A.

2.2 ELM diagnostics

Diagnostic measurements on HL-2A that are capable of sampling during ELM events provide heat flux on the outer divertor target plates, D_α emission in the outer divertor chamber, electron density and temperature in the pedestal, total radiation in the main plasma and the outer divertor region. A poloidal cross section, which shows the locations of these diagnostics and the plasma equilibrium shape used in these experiments, is given in figure 2.

The divertor heat flux is calculated from the evolution of surface temperature on the target plates, measured by an infrared (IR) camera [13]. The infrared camera contains gallium arsenic (GaAs) sensors operating in $8\text{-}9.4\ \mu m$ spectral range, allowing surface temperature from $-40\ ℃$ to $1000\ ℃$ to be measured. An oblong opening on the baffle is cut and thus the outer divertor target plates are monitored directly by the IR camera through a ZnSe vacuum window. Note that there is no inner target IR measurement because viewing is difficult with the very closed

divertor geometry. In order to investigate the characteristics of the ELM power deposition patterns, the IR camera was optimized to have a best field of view covering the strike point zones, and to use a reduced array size with a 4*kHz* sampling rate to resolve the ELMs. Spatial resolution is as small as about *2mm*. Recently, a new $8cm \times 20\,cm$ target graphite tile has taken the place of old copper plates, and a heat transmission layer at the top of the target surface is also introduced in the heat flux calculation [14]. Such developments make it more accurate in the temperature measurement and heat flux calculation. D_α emission in the lower outer divertor is measured with a fast D_α emission detector at a *100 kHz* rate [12].

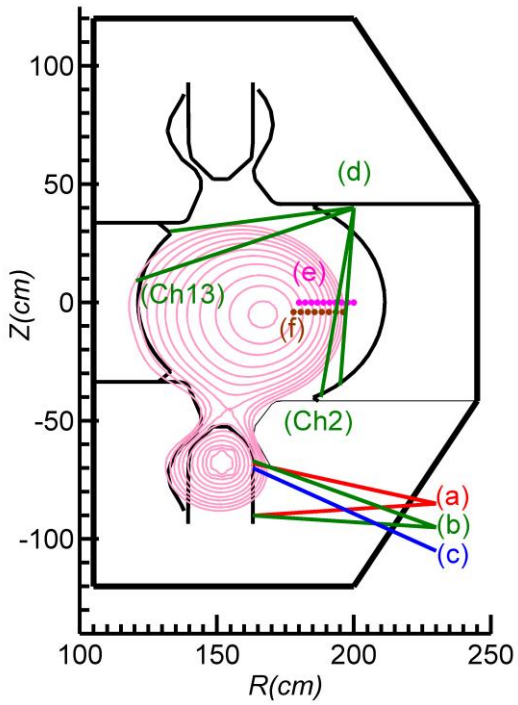

Figure 2. The cross section of HL-2A shows a typical plasma shape used in these experiments and some of the diagnostics used in the ELM analysis. Lines of sight are shown for (a) IR camera, (b) AXUV detector array in the divertor, (c) divertor D_α detectors, (d) AXUV detector array in the main plasma chamber, (e) midplane reflectometers, (f) pedestal ECE. The lines of sight labelled by 'Ch2' and 'Ch13' are used for energy transport in the SOL in figure 7.

Two poloidal arrays of fast AXUV photodiode detectors are applied for estimating the total plasma radiated power during ELMs along multiple chordal views in the main plasma chamber and lower outer divertor. The outer midplane density profile in the SOL and steep gradient region of the pedestal during the ELM cycle is obtained up to $2 \times 10^{19} m^{-3}$ from the X-mode frequency modulated continuous wave (FMCW) reflectometers [15]. The sampling rate of the density profile can be as high as *40 kHz*, while spatial resolution can be as small as *~1cm*. The electron temperature in the pedestal during the ELM cycle is determined by electron cyclotron emission (ECE) radiometer [16]. This system has a tunable local oscillator (LO) source, and can measure the 2^{nd} harmonic ECE frequency from *51* to *142GHz*. The spatial resolution is about *1.5cm* at the toroidal field of *1.3T* and the temporal resolution is about $1\mu s$.

2.3 Experimental data of ELMy H-mode discharges

All results reported in this paper were obtained in deuterium discharges. The lower single null (LSN) divertor configuration with the ion magnetic field gradient drift towards the X-point was used, and a magnetic equilibrium similar to that in figure 2 was optimized for IR measurements of the divertor target power deposition during experiments. Measuring for the inner divertor plates data is not feasible due to the closed divertor geometry, so only the heat load patterns on the outer divertor target are analyzed here.

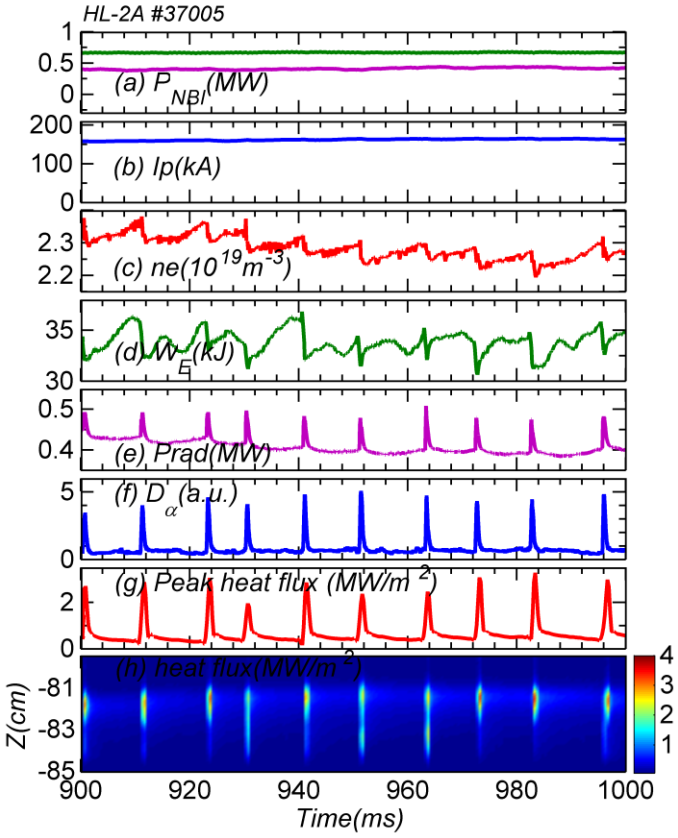

Figure 3. Time traces of the main parameters for one typical HL-2A H-mode discharge: (a) NBI heating power (where NBI#1 in green is about 0.8MW, NBI#2 in purple is about 0.4MW) , (b) plasma current, (c) line-averaged electron density, (d) plasma stored energy, (e) plasma radiation power, (f) divertor D_α signal, (g) peak heat flux, and (h) heat flux on the outer divertor plates (the color represents the value of heat flux in MW/m^2).

Table 1. 30 shots of type-I ELM H-mode discharges with low SOL radiation and attached plasma conditions are chosen for the power load statistical analysis.

I_p (kA)	$B_T(T)$	f_{ELM} (Hz)	$\Delta E/W_{plasma}$(%)	n_e/n_G	P_h(MW)
160-200	1.3-1.5	70-200	3-8	~0.5-0.7	1-1.5

The main parameters for the ELMy H-mode plasmas were $I_p = 160 - 200kA$, $B_t = 1.3 - 1.5T$, and line-averaged electron density $n_e = 2 - 3 \times 10^{19}m^{-3}$. The ELMy H-mode plasmas were achieved with the *1-1.5MW* NBI heating power. A variety of H-mode regimes with different ELM dynamics, including type-I ELMs, type-III ELMs and grass ELMs, were

observed in HL-2A. But in order to compare against other devices, type-I ELMs with frequency from 70 to 2*00Hz* were selected. In this contribution, *30* shots of the so-called IR-optimized ELMy H-mode discharges are chosen for power load analysis due to the combination of the complex viewing geometry, the strike zone positioning and the desired data acquisition with the highest frequency. Some parameters of them are listed in table 1. In addition, the complexity of partially detached divertor plasmas is avoided in this study because IR camera measurement at the target plate is to be meaningfully extrapolated back to the up-stream.

Figure 3 illustrates one typical HL-2A ELMy H-mode discharge. Both divertor plates are attached due to the relatively low plasma density (ne/n_G ~0.6) and the ELM frequency is around 100 Hz and very regular. ELMs cause sudden release of energy and particles from the core plasma, then the power crossing the separatrix is transported by heat conduction and convection along magnetic field lines onto divertor plates. These ELM dynamic characteristics are observed clearly in the line-averaged electron density, plasma stored energy, plasma radiation power, and divertor heat flux, so that heat transport during ELMs and inter-ELMs can be investigated in detail with these diagnostic measurements.

3. Target heat load patterns during ELMs

The spatial and temporal heat flux profiles are determined by the IR thermography, as introduced in section 2. In order to reduce the data scatter, the profiles are obtained by averaging over seven consecutive ELMs with synchronizing the time signal in respect to the start of each single ELM. This method has been described clearly in Ref.17.

3.1. Temporal behaviours

The time period in which an ELM deposits its energy on the divertor target is an important parameter for estimating the material limit. The ELM energy pulse to the divertor target can be divided into two phases (the rise stage and the decay stage) as illustrated in figure 4. The characteristic timescale τ_{rise} for the first phase is defined as the duration of the power increase from 10% above the initial value to 100% of the maximum measured value, and the decay time τ_{decay} for the second phase is the duration from the peak power to 1/e decay [18]. Because τ_{rise} and τ_{decay} cannot be precisely estimated due to the low resampling rate of the IR camera measurement (*~4kHz*), the error bar of about $125\mu s$ (half of frame time) is introduced to determine the upper and lower limits.

In figure 5(a) the power rise and decay times of a total of 30 shots for ELMy discharges with a variety of ELM frequencies are plotted. The observed rise times are in the range between about $200\mu s$ to $400\mu s$, and the decay times are typically 1.5 to 4 times longer than the corresponding rise times. The ELM deposited energy in the power rise and decay phases are estimated with $E = 2\pi R_{div} \iint q(s,t) ds dt$, respectively. The ratio of the deposited energies during two phases varies from 2 to 5, as shown in figure 5(b). In that respect, the fraction of the energy that is deposited during the power rise phase stays below 40%, and can be as low as 20%, although the ELM deposited energy during this phase will lead to the maximum heat flux on the divertor target. These results show a similar tendency with the ELM power load temporal shape report on JET [19]. This means that there is a correlation between the dominant parallel

energy transport mechanism towards the divertor along field lines and the fraction of energy deposited in the first phase of the ELM target heat fluxes. However, the ratio of the ELM deposited energies between two phases shows no dependence on the rise time.

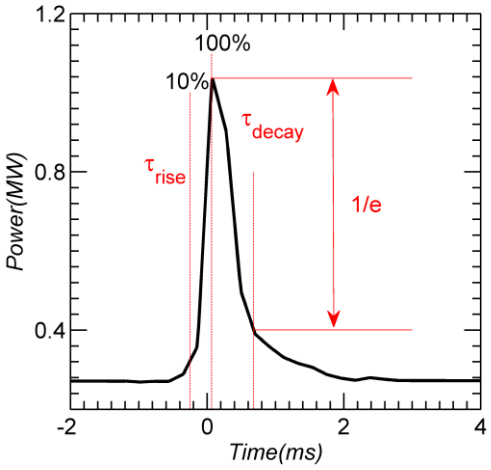

Figure 4. Temporal evolution of outboard deposited power of an averaged ELM event (7 consecutive ELMs). Two phases are determined in the ELM power pulse to the divertor target.

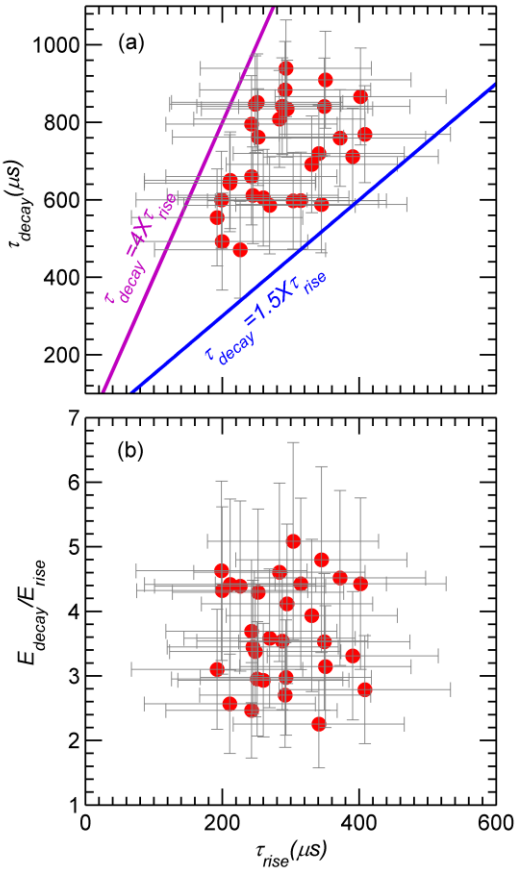

Figure 5. Temporal characteristics of HL-2A Type-I ELMs: (a) ELM decay time versus ELM rise time, (b)Ratio of the ELM energies deposited during decay and rise phases versus ELM

rise time. ELM decay time is much larger than the rise time. ELM energy deposition indicates more energy is deposited in the decay phase.

3.2. ELM power load deposition area

Periodic ELMs induce high transient heat loads onto the divertor targets. In contrast to the very localized steady state heat flux, the ELM heat load is unevenly deposited onto a comparable large area. For the measurement of the impact on the divertor target, the ELM power load deposition area is evaluated in a simple way by dividing the spatially (toroidally and radially) integrated power flux by the peak heat flux [20].

$$A_{wet} = \frac{\int q_{div}(s) 2\pi R_{div} ds}{q_{div}^{max}} \quad (1)$$

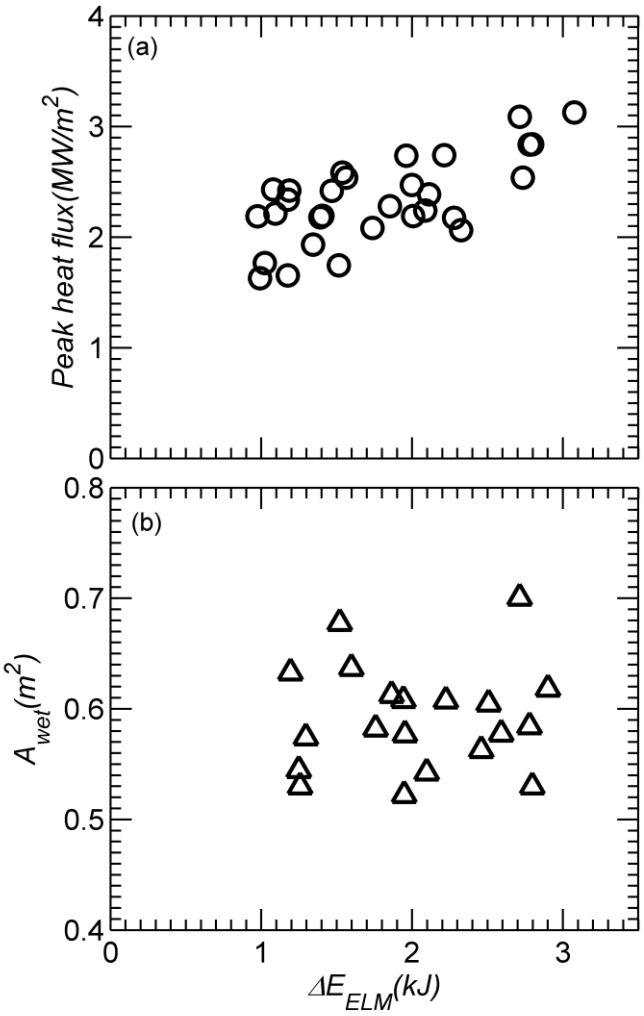

Figure 6. The peak heat flux (a) and the effective wetted area (b) during ELM events versus the ELM energy loss.

In figure 6 the peak heat flux and the wetted area of the ELM peak are plotted. The peak heat flux is estimated by the maximum value of the heat flux profile. The peak value varies from about *1.5MW/m²* to *3.2MW/m²*, which increases with energy loss due to ELMs. The energy loss

due to an ELM is determined by the sharp decrease of plasma stored energy, which is estimated with diamagnetic measurements. It is obvious that, in the attached divertor regime the energy toward divertor will increase with the plasma energy loss, which results in the sharp increase of the peak heat flux. The pitch angle on the target plates is about 2^o near the strike point, so parallel heat flux reaches a value of $q_{\parallel} = \frac{q_{div}}{\sin(\alpha)} = 90\, MW/m^2$. The wetted areas are between 0.5 and 0.7 m^2, and no clear trend of the power broadening scales with the ELM energy loss at this stage.

An integral midplane decay length is estimated with [20]

$$\lambda_{q,midplane} = \frac{A_{wet}}{2\pi R_{div} f_x} \tag{2}$$

here $f_x = \frac{R_{mid} B_\theta^{mid}}{R_{div} B_\theta^{div}}$ is the poloidal magnetic flux expansion at the divertor target. The midplane integral deposited power widths of between 25mm and 40mm are calculated with a value of the effective flux expansion of 1.51, $R_{div} = 1.65m$ for all considered discharges here.

4. Energy transport in the SOL

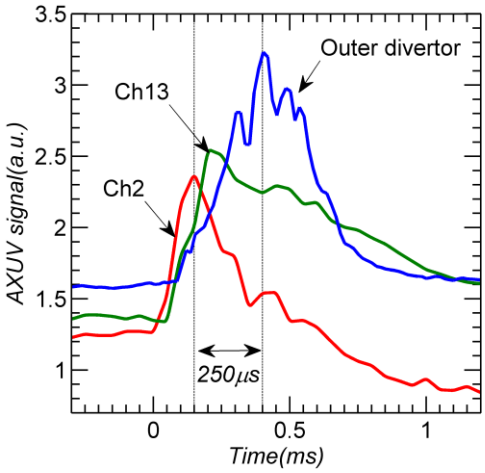

Figure 7. SOL poloidal propagation of ELM radiation pulse from the AXUV detector array analysis. The chordal geometry of the AXUV detector diagnostic and the lines of sight used in the analysis are defined in the figure 2.

An important aspect of the mechanism that governs the power deposition onto the target plates is the characteristic time of SOL energy transport by ELMs to the divertor. The characteristic time is estimated as collisionless transport of ions with the sound speed [18]:

$$\tau_{\parallel}^{ELM} = \frac{2\pi qR}{\sqrt{(T_e + T_i)/m_d}} \tag{3}$$

assuming $T_e = T_i = T_{ped}$, T_{ped} is the pedestal values of electron temperature and m_d the mass of the deuterium ions. For a typical ELMy H-mode discharge in HL-2A, a connection length of about $L = 2\pi qR = 51m$ and a pedestal temperature of about $T_{ped} = 0.4keV$,

resulting in a $\tau_{\parallel}^{ELM} = 261\mu s$. The timescale is confirmed by the AXUV detector array data, as shown in figure 7. The radiation peak presents first in the low field side of the plasma and then in the high field side and finally in the outer divertor. These observations are consistent with SOL parallel transport from the outer midplane. The timing of the ELM induced radiation perturbation at various poloidal locations is about *250μs* as shown in figure 7, in good agreement with ion convection parallel to SOL filed lines from the midplane to the target plates.

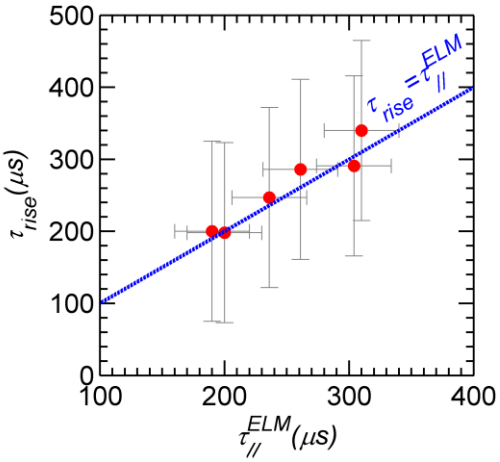

Figure 8. The ELM power rise time measured by the IR thermography is compared to the parallel transport time of ions calculated from pedestal electron temperature.

The timescale τ_{rise} (see figure 4) of the power deposition on the divertor target is correlated with the collisionless flight time $\tau_{\parallel}^{ELM}$ of the pedestal energy ions to the divertor, as shown in figure 8. Note that $\tau_{\parallel}^{ELM}$ contains only the pedestal top electron temperature and a characteristic length. The good correlation of $\tau_{\parallel}^{ELM}$ with τ_{rise} suggests that convective transport along open field lines towards the divertor target dominates the parallel heat transport mechanism during ELMs. The results are consistent with the reports on the JET [21]

5. ELM energy fluence scaling

5.1 Eich model

The peak of the ELM energy fluence profile directly relate to the material limit, which should be limited to $0.5MJ/m^2$ to prevent edge melting. The ELM energy fluence profile, $\varepsilon_{\parallel}(s)$, is the temporal integration of the ELM heat flux profiles over the ELM duration (defined in section 3).

$$\varepsilon_{\parallel}(s) = \int_{t_{ELM}} q_{\parallel}(s,t)dt \tag{4}$$

$$q_{\parallel}(s,t) = \frac{q_{div}(s,t) - q_{div}(s,t_0)}{\sin(\alpha_{div})} \tag{5}$$

$$\varepsilon_{\parallel}^{peak} = \max(\varepsilon_{\parallel}(s)) \tag{6}$$

The heat flux, $q_{div}(s,t)$, is measured by the IR thermography, and subtracted by the heat flux just before the ELM, $q_{div}(s,t_0)$. S is the local coordinate along the tile surface. Figure 9 shows an example of time evolutions of the ELM heat flux profiles during an ELM event, and the ELM target energy fluence profiles for 7 individual ELMs.

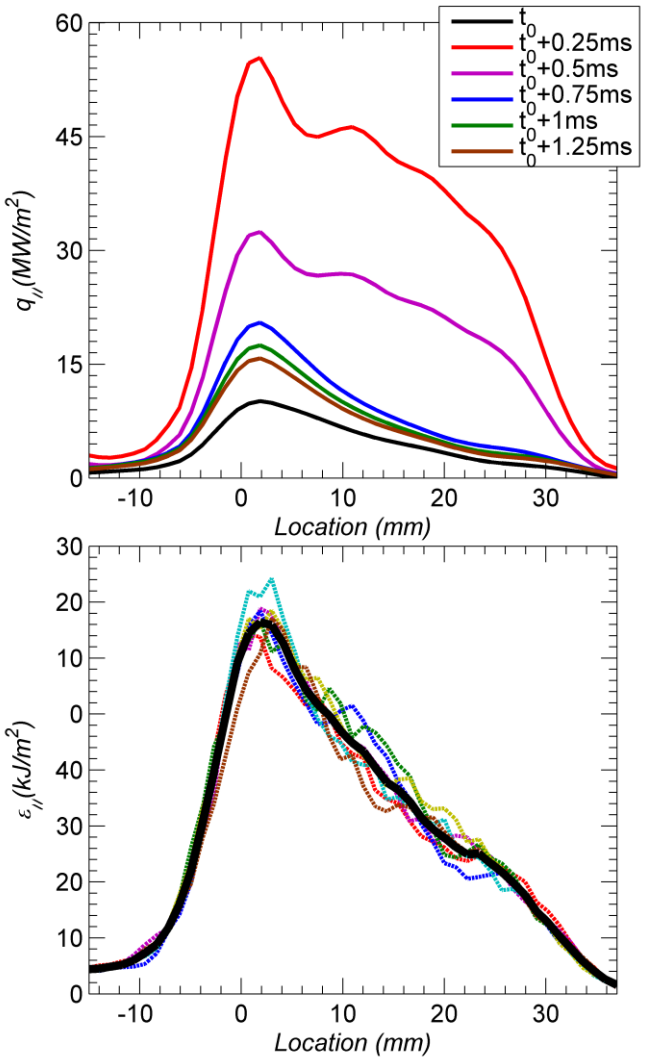

Figure 9. Evolutions of heat flux profiles during an ELM event (a) and examples of ELM energy density profiles for 7 individual ELMs on the outer divertor targets. The averaged profile (black line) is used for the ELM energy fluence scaling.

The Eich model provides predictions for the ELM heat loads, which are compared against a multi-machine dataset [9]. The model assumes a direct flux tube connection between the pedestal top and the divertor during an ELM, and the width of the flux tube around the pedestal top position determines the deposition area in the divertor. As mentioned in section 4, the parallel heat transport along open field lines dominates the transport mechanism during ELMs, so the assumption is valid for the HL-2A database. Based on the assumptions, the ELM parallel peak energy fluence is well described by the pedestal top pressure [9]

$$\varepsilon_{\parallel} \cong 6\pi P_e R_{geo} q_{edge} \quad (4)$$

Where $P_e = n_{e,ped,top} T_{e,ped,top}$ is the plasma pressure around the pedestal top region, $q_{edge} = \sqrt{\frac{1+\kappa^2}{2}} \cdot \frac{a_{geo}}{R_{geo}} \cdot \frac{B_{tor}}{B_{pol}}$ is the edge cylindrical safety factor, R_{geo} and a_{geo} are the geometrical major radius and minor radius, and B_{tor} and B_{pol} are the toroidal and poloidal magnetic field at the outer midplane.

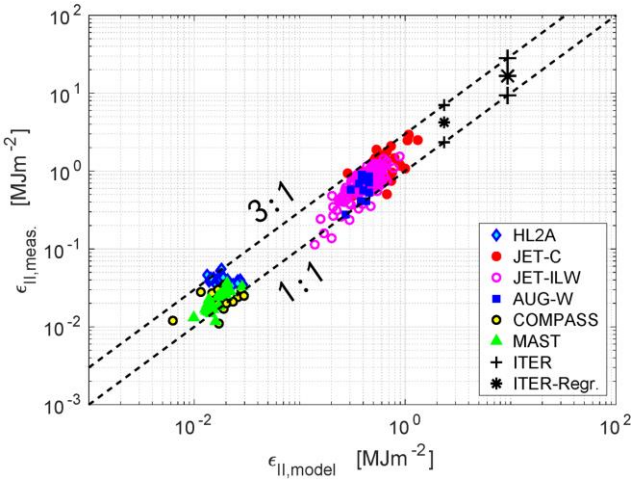

Figure 10. Model prediction versus the data base. For comparison, the data from other devices are also shown. The dashed lines are one and three times the model prediction respectively.

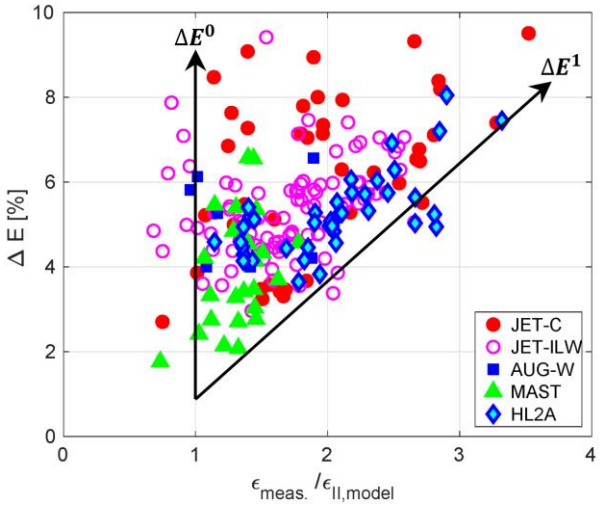

Figure 11. The distribution of the relative ELM size versus the measured parallel ELM energy fluence normalized to the model prediction.

5.2 ELM energy fluence scaling

The comparison of the experimental HL-2A data and the Eich model prediction is shown in figure 10. For comparison, the data of multi-machines are also given out in the figure [9]. The experimental data range is found to lie between one and three times the model prediction, showing a good agreement with other device data. The dashed lines in figure 10 are one and

three times the model prediction, and the range between two lines is possibly related to the relative ELM size. The relative ELM size is defined as the ELM loss energy normalized to the plasma stored energy $\Delta E = E_{loss}/W_{plasma}$, which is calculated by using diamagnetic measurements on the plasma stored energy at the beginning and the end of the ELM event. Figure 11 shows the measured parallel ELM energy fluence normalized to the model prediction versus the relative ELM size. It can be seen that the data almost fill in the region of between the 1:1 line and 3:1 line, data close to the 3:1 line are rare and existent only for large ELMs with relative ELM size at about 7-9%. However, there is a significant scatter in the HL-2A dataset. It should be noted that the HL-2A tokamak is operated with very closed divertor geometry compared with other open divertor geometries. This maybe causes the significant scatter. In addition, the distribution of multi-machines database demonstrates a relationship of the parallel ELM energy fluence and the relative ELM size, $\varepsilon_{\parallel} \sim \Delta E^{\alpha}$ with α being between 0 and 1, which is consistent with the regression studies report of $\varepsilon_{\parallel} \sim \Delta E^{0.5}$ [9].

6. Summary and conclusions

A set of ELMy H-mode discharges has been optimized for the ELM energy deposition studies. Insight into the temporal or spatial evolution of the ELM structure is gained by a statistical analysis of the amplitudes and spatial distribution of the pattern on the divertor targets. The ELM energy loss in HL-2A is about 3%-8% of the plasma stored energy, and the corresponding peak heat flux and the integrated power decay length are in the range of *1.5-3.2MWm*$^{-2}$ and *25-40mm*, respectively. The effect of ELMs on the peak heat flux is larger than that on the decay length, because the peak heat flux increases by a factor of 1.5-5.5 while the decay length increases only by a factor of 1-2 compared with the values in between ELMs. In addition, the peak heat flux increases with the energy loss due to an ELM, but the decay length shows no dependence on that.

Since the ELM power rise time scales with the convective parallel time, ELMs are expected to have main convective transport properties. A delay in the response of the divertor plasma radiation of the ELM perturbation relative to pedestal radiation is observed as expected for the convective transport of energy. But a characterization of the ELM pedestal losses separately in temperature and density has revealed both conductive as well as convective ELM losses for DIII-D [22], JET [23] and ASDEX Upgrade [24]. Hence, the temperature and density profiles at the midplane and the divertor should be taken into account for further studies. However, the ratio of the ELM energies deposited in the rise and decay phases varies from 20% to 50%, which is consistent with other devices [18], and thus more energy is deposited in the decay phase.

The convective transport along open field lines towards the divertor target dominates the parallel heat transport mechanism during ELMs. This observation supports the Eich model assumption of a direct flux tube connection between the pedestal top and the divertor during an ELM. Finally, ELM energy density, $\varepsilon_{\parallel}$, profiles are compared with the predictions of the model [9], and it shows a good agreement between experimental and predicated values.

Acknowledgements

This work was supported by National Key R&D Program of China under Grant Nos. 2018YFE0303101, 2017YFE0301106, 2017YFE0301202 and 2018YFE0310300, and Natural Science Foundation of China under Grant Nos.11875020 and 11875023.

References

[1] Pitts R.A. et al., 2019 Nuclear Materials and Energy 20 100696
[2] Wagner F. et al., 1982 Phys. Rev. Lett. 49 1408
[3] Zohm H. 1996 Plasma Phys. Control. Fusion 38 105
[4] Sieglin B. 2017 Phys. Scr. T170 014071
[5] Silburn S.A. 2017 Phys. Scr. T170 014040
[6] Eich T. et al., 2005 Plasma Phys. Control. Fusion 47 815
[7] Fenstermacher M.E. et al., 2003 Plasma Phys. Control. Fusion 45 1597
[8] Wang L. et al., 2013 Nucl. Fusion 53 073028
[9] Eich T. et al., 2017 Nuclear Material and Energy 12 84-90
[10] Adamek J., et al., 2017 Nucl. Fusion 57 116017
[11] Knolker M., et al., 2018 Nucl. Fusion 58 096023
[12] Duan X.R. et al., 2010 Nucl. Fusion 50 095011
[13] Gao J.M. et al., 2013 Chin. Phys. B 22 015202
[14] Eich T. et al., 2007 Plasma Phys. Contr. Fusion 49 573
[15] Zhong W.L. et al., 2014 Rev. Sci. Instrum. 85 013507
[16] Shi Z.B. et al., 2014 Rev. Sci. Instrum. 85 023510
[17] Pitts R.A. et al., 2003 Nucl. Fusion 43 1145.
[18] Eich T. et al., 2005 J. Nucl. Mater. 337-339 669
[19] Eich T. et al., 2011 J. Nucl. Mater. 415 S856
[20] Loarte A. et al., 1999 J. Nucl. Mater. 266-269 587
[21] Loarte A. et al., 2004 Phys. Plasma 11 2668.
[22] Leonard A. et al., 2002 Plasma Phys. Contr. Fusion 44 945
[23] Loarte A. et al., 2003 Plasma Phys. Contr. Fusion 45 1549
[24] Urano H. et al., 2003 Plasma Phys. Contr. Fusion 45 1571